



Universiteit
Leiden
The Netherlands

Multimodal image-guided interventions using oncological biomarkers

Stammes, M.A.

Citation

Stammes, M. A. (2018, May 22). *Multimodal image-guided interventions using oncological biomarkers*. Retrieved from <https://hdl.handle.net/1887/62351>

Version: Not Applicable (or Unknown)

License: [Licence agreement concerning inclusion of doctoral thesis in the Institutional Repository of the University of Leiden](#)

Downloaded from: <https://hdl.handle.net/1887/62351>

Note: To cite this publication please use the final published version (if applicable).

Cover Page



Universiteit Leiden



The handle <http://hdl.handle.net/1887/62351> holds various files of this Leiden University dissertation.

Author: Stammes, M.A.

Title: Multimodal image-guided interventions using oncological biomarkers

Issue Date: 2018-05-22



Chapter 6

Pre-clinical evaluation of a cyanine based SPECT probe for multimodal tumor necrosis imaging

Marieke A. Stammes, Vicky T. Knol-Blankevoort, Luis J. Cruz, Hans R.I.J. Feitsma, Laura Mezzanotte, Robert A. Cordfunke, Riccardo Sinisi, Elena A. Dubikovskaya, Azusa Maeda, Ralph S. DaCosta, Katja Bierau, Alan B. Chan, Eric L. Kaijzel, Thomas J.A. Snoeks, Ermond R. van Beek, Clemens W.G.M. Löwik.

Adapted from: Pre-clinical evaluation of a cyanine based SPECT probe for multimodal tumor necrosis imaging, *Mol Imaging Biol.* 2016 Dec; 18(6): 905-915

Abstract

Purpose

Recently we showed that a number of carboxylated near infra-red fluorescent (NIRF) cyanine dyes possess strong necrosis avid properties *in vitro* as well as in different mouse models of spontaneous and treatment induced tumor necrosis, indicating their potential use for cancer diagnostic- and prognostic purposes. In the previous study, the detection of the cyanines was achieved by whole body optical imaging, a technique that, due to the limited penetration of near-infra red light, is not suitable for investigations deeper than one centimeter within the human body. Therefore, in order to facilitate clinical translation, the purpose of the present study was to generate a necrosis avid cyanine based probe that could be used for Single Photon Emission Computed Tomography. For this, the necrosis avid NIRF cyanine HQ4 was radiolabeled with ^{111}In Indium, via the chelate diethylene triamine pentaacetic acid (DTPA).

Procedures

The necrosis avid properties of the radiotracer [^{111}In]DTPA-HQ4 were examined *in vitro* and *in vivo* in different breast tumor models in mice using SPECT and optical imaging. Moreover, biodistribution studies were performed to examine the pharmacokinetics of the probe *in vivo*.

Results

Using optical imaging and radioactivity measurements, *in vitro*, we showed selective accumulation of [^{111}In]DTPA-HQ4 in dead cells. Using SPECT and in biodistribution studies, the necrosis avidity of the radiotracer was confirmed in a 4T1 mouse breast cancer model of spontaneous tumor necrosis and in a MCF-7 human breast cancer model of chemotherapy-induced tumor necrosis.

Conclusions

The radiotracer [^{111}In]DTPA-HQ4 possessed strong and selective necrosis avidity *in vitro* and in various mouse models of tumor necrosis, indicating its potential to be clinically applied for diagnostic purposes and to monitor anti-cancer treatment efficacy.

Introduction

Necrosis is a form of cell death characterized by severe cell swelling, denaturation and coagulation of cytoplasmic proteins and disruption of the cell membrane, causing the release of its intracellular content. Necrotic cell death is irreversible and is induced by external factors or disease, such as radiation, trauma and loss of blood supply, and is also involved in cancer development and treatment^{1,2}. In the center of most solid tumors, an area of ischemia and subsequent necrosis develops, as vascularization cannot keep up with the rapidly growing tumor mass. The size and growth rate of this necrotic area is positively correlated with the aggressiveness of cancer and can, therefore, be used as a diagnostic biomarker of cancer staging³⁻⁸. Moreover, anti-cancer treatments like chemotherapy are utilized to induce cell death, increasing the total amount of tumor necrosis⁹⁻¹¹. Thus, agents that specifically bind to necrotic tumor tissue can contribute to a more accurate disease diagnosis and can be exploited to predict early treatment outcome of anti-cancer treatments¹². To this end, back in 1988, Epstein and colleagues¹³ developed so called Tumor Necrosis Targeting (TNT) antibodies, that are directed towards nuclear proteins, and labeled with radioactive Iodine for imaging and anti-cancer treatment purposes. Likewise, the photosensitizing agent Hypericin has also been shown to possess necrosis avidity and is currently under investigation for cancer imaging and treatment purposes¹⁴⁻¹⁷. However, there are several drawbacks for the existing agents. Antibodies are relatively large in size, have long circulation time, could induce immune response and expensive to develop in Good Manufacturing Practices (GMP) quality, and the photosensitizer Hypericin is phototoxic, poorly soluble and tend to aggregate rapidly^{16,18,19}. All these issues hamper the clinical translation of these compounds^{14,20-22}.

Recently, we reported on two near infrared fluorescent (NIRF) carboxylated cyanine dyes, HQ5 and IRDye 800CW (800CW) that also possess strong necrosis avid properties²³. Cyanines are, amongst other dyes, widely used as fluorescent tags for protein labeling to enable whole body optical imaging in small animals²⁴⁻²⁸. Although the mechanism of necrosis avidity is not fully understood, it is independent on the Enhanced Permeability and Retention (EPR) effect^{23,29}. On a cellular level, increased retention of the dye may involve augmented accessibility to cells that have lost membrane integrity along with an increased affinity to denatured cytoplasmic proteins³⁰⁻³². Using whole body optical imaging in mice, we showed that these cyanines can

be employed to image areas of spontaneous necrosis in solid tumors and to determine the efficacy of chemotherapy by monitoring therapy-induced tumor necrosis²³.

Optical imaging is successfully applied in whole body imaging for small animals and in imaging of superficial tissues in humans. Optical imaging is based on the detection of light emitted from agents and/or tags coupled to biomolecules in living systems. In order to obtain better tissue penetration, optical imaging often makes use of agents and tags that emit light in the near infrared range. However, even with these compounds, the maximal penetration depth is limited to a few cm^{33,34}. Although, this relatively small measuring range is sufficient for the detection of light in small animals, it is not sufficient for the detection of light in deep tissues such as tumors situated deep within the human body. Alternatively, nuclear imaging modalities such as Single Photon Emission Computed Tomography (SPECT) and Positron Emission Tomography (PET) are used clinically to image deep tissues. To enable SPECT and/or PET imaging for clinical translation, our previously described necrosis avid NIRF cyanines must be radiolabeled. Generally, this is achieved by conjugating a targeting moiety to a chelate that is subsequently labeled with a metal radionuclide³⁵⁻³⁸. In the present study we employed this principle to the necrosis avid cyanine HQ4, a close structural analogue of the recently studied necrosis avid cyanine HQ5²³. As HQ5 has two moieties which can be functionalized by the chelate diethylene triamine pentaacetic acid (DTPA) we used HQ4, a mono-derived analogue, to avoid scrambling of the DTPA molecules or steric hindrance³⁹. HQ4 was conjugated to the chelate (DTPA) and subsequently labeling with ¹¹¹Indium-chloride (¹¹¹In-Cl₃) was performed. In this study we investigated the necrosis avidity of [¹¹¹In]DTPA-HQ4 *in vitro* and in mouse tumor models of spontaneous and chemotherapy induced tumor necrosis using optical imaging and SPECT.

Material and methods

Compounds

The cyanine dyes; HQ4 carboxylate and HQ4-NHS ester were obtained from Ilumicare BV (Rotterdam, The Netherlands).

Synthesis of HQ4-DTPA

Synthesis of diethylene triamine pentaacetic acid (DTPA)- Polyethylene Glycol (PEG) -NH₂, DTPA containing PEG amine link (4,7,10-trioxa-1,13-tridecanediamine, indicated as PEG-NH₂ in the formula (DTPA-PEG-NH₂) was synthesised on Chloride-Trityl Chloride (Cl-TrtCl) resin. Thus, Fluorenylmethoxycarbonyl (Fmoc)-PEG amine was incorporated on Cl-TrtCl resin (CTC resin) by reacting 3eq. Fmoc-PEG amine in presence of 6eq. N,N-Diisopropylethylamine (DIEA) in Dichloromethane (DCM) overnight at room temperature (RT). Final loading was measured by Fmoc quantification and the value obtained was around 0.8 mmol/g. Fmoc group removal was carried out with piperidine— Dimethylformamide (DMF) (1:5)(1 x 1min, 2 x 10min). Next, the DTPA-(*tert*-tBu ester)-COOH (2eq.) was coupled using N,N'-dipropan-2-ylmethanediiimine (DIPCDI) (2eq.) and Hydroxybenzotriazole (HOBt) (2eq.) in DMF overnight. After coupling overnight the ninhydrin test was negative. Later on, DTPA-(*tert*-tBu ester)-CO-NH-PEG-CTC-resin cleavage and deprotection was performed in two steps. DTPA-(*tert*-tBu ester)-CO-NH-PEG-CTC-resin was treated with 1% Trifluoroacetic acid (TFA) in DCM 10 times for 1min each time. Excess DCM was removed using vacuum and side chain protecting groups were removed using 95% TFA, 2.5% Triisopropylsilane (TIS) and 2.5% water. DTPA-CO-NH-PEG-NH₂ was precipitated with cold Methyl-*tert*-butylether (MTBE) after TFA removal under a N₂ stream. The DTPA-CO-NH-PEG-NH₂ was dissolved in water and lyophilized to obtain the final product. The desired DTPA-CO-NH-PEG-NH₂ was 85.0% in yield with a purity of 90.6% as analyzed by High-performance liquid chromatography (HPLC) (retention time 2.28min). HPLC- mass spectrometry (MS), m/z calc.: 523.25 for C₂₀H₃₇N₅O₁₁, Found: 524.5.28 [M+1]⁺ and matrix assisted laser desorption/ionisation time-of-flight (MALDI-TOF) analysis found 524.2 [M+1]⁺ 546.3 [M+Na].

Synthesis of DTPA-CO-NH-PEG-NH₂-HQ4: HQ4-NHS (8.3x10⁻⁴mmol, 1 mg) dissolved in 50μL of Dimethyl sulfoxide (DMSO) was added to DTPA-CO-NH-PEG-NH₂ (2.8 x 10⁻³mmol, 2mg) dissolved in 200 μL of DMSO containing 5μL DIEA and stirred overnight at room temperature. Later on, the complex DTPA-CO-NH-PEG-HQ4 was purified by reversed phase (RP)-HPLC. The desired DTPA-

PEG-HQ4 was 50.5% in yield with a purity of 98% as analyzed by HPLC (tR 5.34). HPLC-MS, m/z calc.: 1331.59 for C₆₆H₉₀N₈O₁₇S₂, Found: 1332.0[M+1]⁺ and MALDI-TOF Found 1331.9 [M+1]⁺ 1353.9 [M+Na].

Cells and culture conditions

4T1-luc2 mouse mammary cancer cells (PerkinElmer, Waltham, MA, USA) and, MCF-7 human mammary cancer cells were all cultured in RPMI-1640 medium (Life Technologies Inc., Carlsbad, CA, USA) supplemented with 10% fetal calf serum (FCS; Lonza, Basel Switzerland), 100 units/ml penicillin and 50 µg/ml Streptomycin (Life Technologies Inc.). All cell lines were cultured in a humidified incubator at 37°C and 5% CO₂, monthly checked for Mycoplasma infection by polymerase chain reaction (PCR) and checked routinely for morphologic changes.

Dry ice dead cell assay

In vitro, cell death was studied using a cryo-induced cell death assay as previously described⁴⁰. In short, 4T1-luc2 cells were seeded onto 24-well tissue culture plates (Sigma-Aldrich) and grown until confluent. After discarding the medium, a bar of dry ice 3-5mm in diameter was applied to the underside of the culture well for 20sec. Subsequently, the cells were incubated in the dark for 15min. at RT with HQ4 at a concentration of 100 nM. After incubation, the samples were gently washed with phosphate buffered saline (PBS) and subsequently scanned for fluorescence using the Odyssey Infrared Imager 9120 (LI-COR) and for radioactivity via phosphor imaging on the Typhoon 9410 imager (GE Healthcare).

***In vitro* viability assay**

4T1-luc2 cells were plated in a 96-well plate (Costar) in 100 µl medium at a density of 10.000 cells per well and left over night to adhere. The next day the medium was replaced with medium containing the experimental compounds: HQ4, HQ4-DTPA, HQ5 and Gambogic acid (GA), 3 wells per condition. After 24h, cell viability was measured using a nonradioactive colorimetric MTS viability assay (Promega Benelux) according to the manufacturer's protocol. Optical absorption was measured at 490 nm with a Versamax absorbance microplate reader (Molecular Devices).

Animals

Female athymic mice (BALB/c nu/nu, 6 weeks old) were purchased from Charles River Laboratories (L'Arbresle Cedex, France). Animals were housed at 22°C and 50% humidity with free access to food and water and maintained under standard 12 h light/12 h dark cycles. All surgical and analytical procedures were performed under isoflurane gas anesthesia (3% induction, 1.5-2% maintenance) in 70% pressurized air and 30% O₂. Animals were sacrificed by cervical dislocation at the end of the experimental period. The animals were housed per 4-5 animals in individually ventilated cages with ad libitum access to food and water.

All animal experiments were assessed for animal health, ethics, and research and approved by the Animal Welfare Committee of Leiden University Medical Center, the Netherlands. All mice received humane care and were kept in compliance with the Code of Practice Use of Laboratory Animals in Cancer Research (Inspectie W&V, July 1999).

Subcutaneous Tumor Model

Approximately 1×10^5 4T1-luc2 cells, suspended in 15 μ l PBS, were implanted bilateral and subcutaneously onto the upper back of nude mice. Tumors were grown until they reached a size of 6-7 mm in diameter which developed roughly after 1.5-2 weeks of tumor implantation.

Similarly, 2×10^6 MCF-7 cells, suspended in 15 μ l PBS in a 1:1 mixture with 15 μ l of Matrigel (BD biosciences, San Jose, CA, USA) were injected bilateral and subcutaneously onto the upper back. Tumors were grown until they reached 6-7 mm diameter, which developed after approximately 2-3 weeks.

Whole body FLI measurements were performed using the Pearl Impulse *in vivo* fluorescence imager (LI-COR) and/or IVIS Spectrum *in vivo* imaging system (PerkinElmer) several time points after injection. On the IVIS, an excitation and emission wavelength of 675nm and 720 nm was used for HQ4.

Radiolabeling of HQ4-DTPA and SPECT

To label HQ4-DTPA with $^{111}\text{In-Cl}_3$, it was dissolved in 0.1M Hepes (10 μ g/100 μ l) and $^{111}\text{In-Cl}_3$ (35MBq; Covidien-Mallinckrodt, Dublin, Ireland) was added. After 30min. of incubation on the shaker, labeling was validated with high-pressure liquid chromatography (HPLC) (Jasco Inc., Easton, MD, USA) or thin layer chromatography (TLC). In all cases, labeling efficacy was >90%.

To study the specificity of the radiolabeled HQ4-DTPA versus radiolabeled DTPA *in vivo*, 10 μ g [^{111}In]DTPA-HQ4 (=10 nmole per mouse) or 10 μ g

[¹¹¹In]DTPA was injected i.v. into mice bearing 4T1-luc2 tumors (n=3 and 4, respectively). The total injected dose (ID) in each mouse was determined in a dose-calibrator (VDC101, Veenstra Instruments, Joure, the Netherlands).

SPECT scans were conducted at several time points post injection on a 3-headed U-SPECT-II gamma camera (MILabs, Utrecht, The Netherlands) under isoflurane anesthesia for 40 minutes. Radioactivity counts from total body scans were acquired using a 0.6mm mouse pinhole collimator with energy settings at 171 and 245keV with a window of 20% and background energy settings of respectively 4.5% and 3.5% around the tails of the energy window⁴². Subsequently, the image was reconstructed using 20 POSEM iterations with 4 subsets, 3D gauss 1 mm (FWHM) filtering, a 0.2mm voxel size, and with decay and scatter corrections integrated into the reconstruction⁴³. Images were generated and analyzed using PMOD software. *In vivo* SPECT scanning was followed by *in vivo* fluorescence imaging on the Pearl Impulse Small Animal Imaging System (LI-COR).

After the last imaging time point mice were sacrificed and several tissues were excised, weighed, and counted for radioactivity (Wizard2 2470 automatic gamma scintillation counter, Perkin Elmer, USA) to determine the percentage of the injected dose per gram (%ID/g). The %ID/g was calculated as follows: ((MBq measured in tissue/injected dose) *100%) /weight of tissue).

Chemotherapy of MCF-7 tumors

In two groups of mice (n=5), two weeks after tumor implantation the mice received either an i.p. injection of cyclophosphamide (265 mg/kg; Baxter BV, Utrecht, The Netherlands)⁴⁴ or remained untreated. After 72hr, all animals received an i.v. injection of radiolabeled HQ4-DTPA. SPECT scans were conducted 24hr later, followed by whole body FLI. After the last imaging time point mice were sacrificed, several tissues were excised, weighted, and counted for radioactivity.

***Ex vivo* tumor imaging**

Ex vivo tumor imaging was performed to visualize the distribution of the probe in the tumor. Images were obtained for FLI (Odyssey Infrared Imager 9120 (LI-COR)) and for radioactivity via phosphor imaging (Typhoon 9410 imager (GE Healthcare) and ImageQuant TL software). For phosphor imaging the tumors were manually sliced in sagittal sections and placed o/n on a phosphorscreen.

Histological procedures

The tumors collected for histological analysis were fixed in 4% formaldehyde and embedded in paraffin. 5µm sections were prepared and FLI was performed using the Odyssey Infrared Imager (LI-COR). Afterwards, the sections were subjected to TdT-mediated dUTP Nick-End Labeling (TUNEL) staining (Promega, Madison, WI, USA) to validate accumulation of the NIRF probes in necrotic cells.

Statistical Analysis

All statistical analyses was performed using Prism software (GraphPad). For repeated measures a student's t-test was used in all cases. $P < 0.05$ was considered significant, and all error bars represent mean \pm SEM.

Results

We selected the necrosis avid cyanine HQ4, instead of HQ5, to perform radiolabeling and further *in vitro* and *in vivo* investigations to demonstrate its potential clinical translation. The choice for HQ4 was based on the number of functionalized moieties present in the cyanine molecules, which is one in the case of HQ4 and two in the case of HQ5 (see **Fig. 1A**). Furthermore, as shown in **Figure 1B**, HQ4 showed slightly higher necrosis avid properties in our dry ice dead cell assay than HQ5. The fluorescent signal intensity, obtained from the area of cell death caused by freezing, was over the whole dose range (1 -100 nM) 2.8 (+/- 1.0) -fold higher for HQ4 as compared to HQ5. A HQ4-DTPA hybrid complex was synthesized by covalent coupling via conjugation with a polyethylene glycol (PEG) linker (**Fig. 2**).

Reversed-phase chromatography showed a clear peak indicating the high grade of purity (98%) of this conjugate. Mass spectrometric analysis of HQ4-DTPA further showed the expected molecular weight (calc.: 1331.59 for $C_{66}H_{90}N_8O_{17}S_2$ and MALDI-TOF found 1332.4 [M+1]⁺ 1354.6 [M+Na]), indicating the high grade of purity of this conjugate (see **Fig. 3**). Lastly, the HQ4-DTPA conjugate was labeled with $^{111}\text{In-Cl}_3$ with a labeling efficiency of >90% (data not shown).

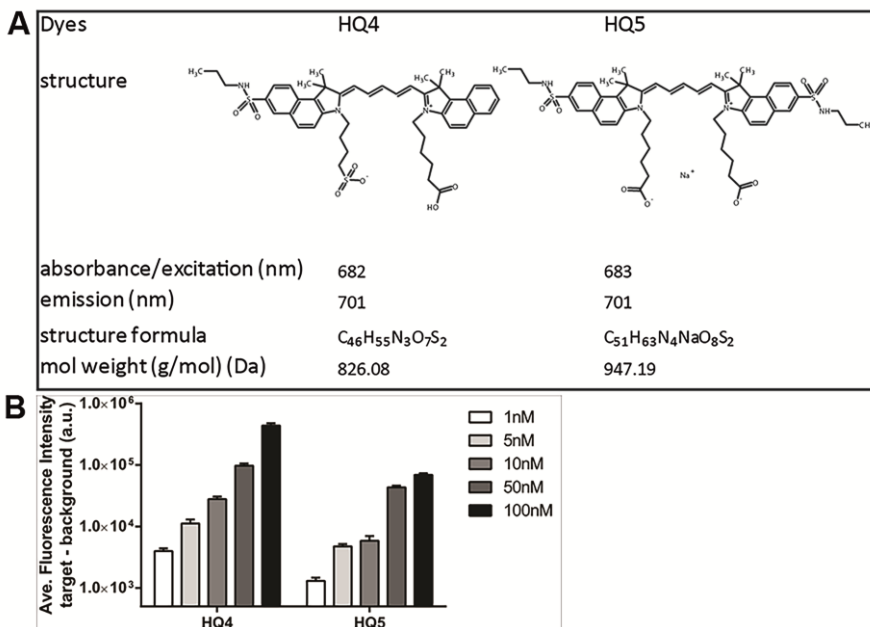


Figure 1. Structural characteristics and *in vitro* necrosis avid properties of HQ4 vs HQ5.

(A) Chemical and structural characteristics of the carboxylated cyanine dyes HQ4 and HQ5.

(B) *In vitro* necrosis targeting properties of HQ4 and HQ5 utilizing the dry ice assay. Fluorescent signal intensity was obtained from the area of dead cells in the center of a culture well after incubation with different concentrations of HQ4 or HQ5 (1-100 nM) and is subtracted by the background signal from the area of the living cells.

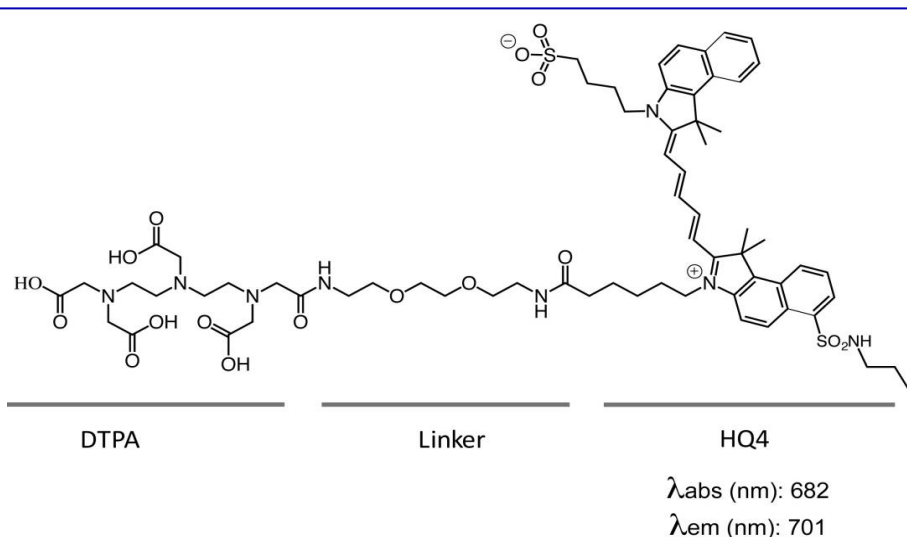


Figure 2. Chemical and structural characteristics of HQ4-DTPA.

Chemical structure of HQ4-DTPA. λ_{obs} =absorbance wavelength; λ_{em} =emission wavelength.

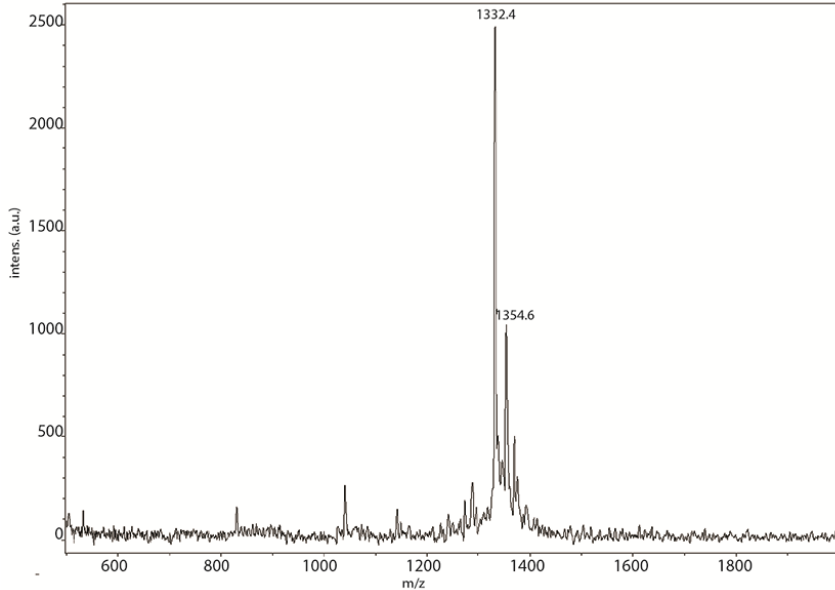


Figure 3. Reversed-phase mass spectrometry of HQ4-DTPA.

Reversed-phase chromatography showed a clear peak indicating the high grade of purity (98%) of this conjugate. Mass spectrometric analysis of HQ4-DTPA further showed the expected molecular weight (calc.: 1331.59 for $C_{66}H_{90}N_8O_{17}S_2$ and MALDI-TOF found 1332.4 $[M+1]^+$ 1354.6 $[M+Na]^+$), indicating the high grade of purity of this conjugate.

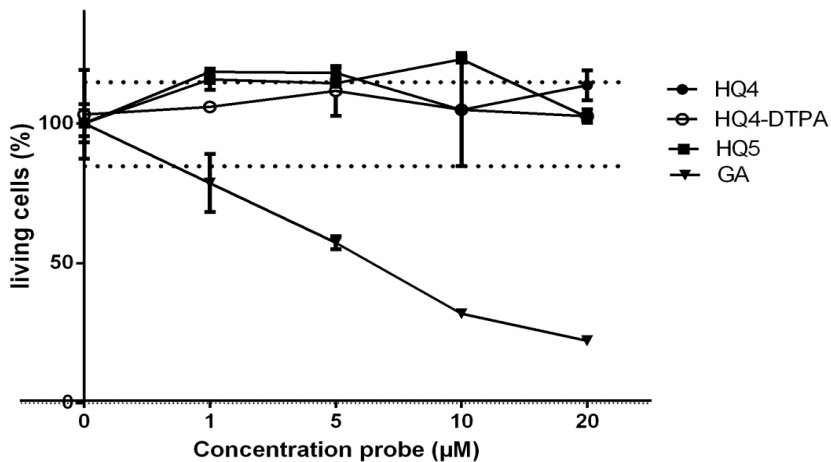


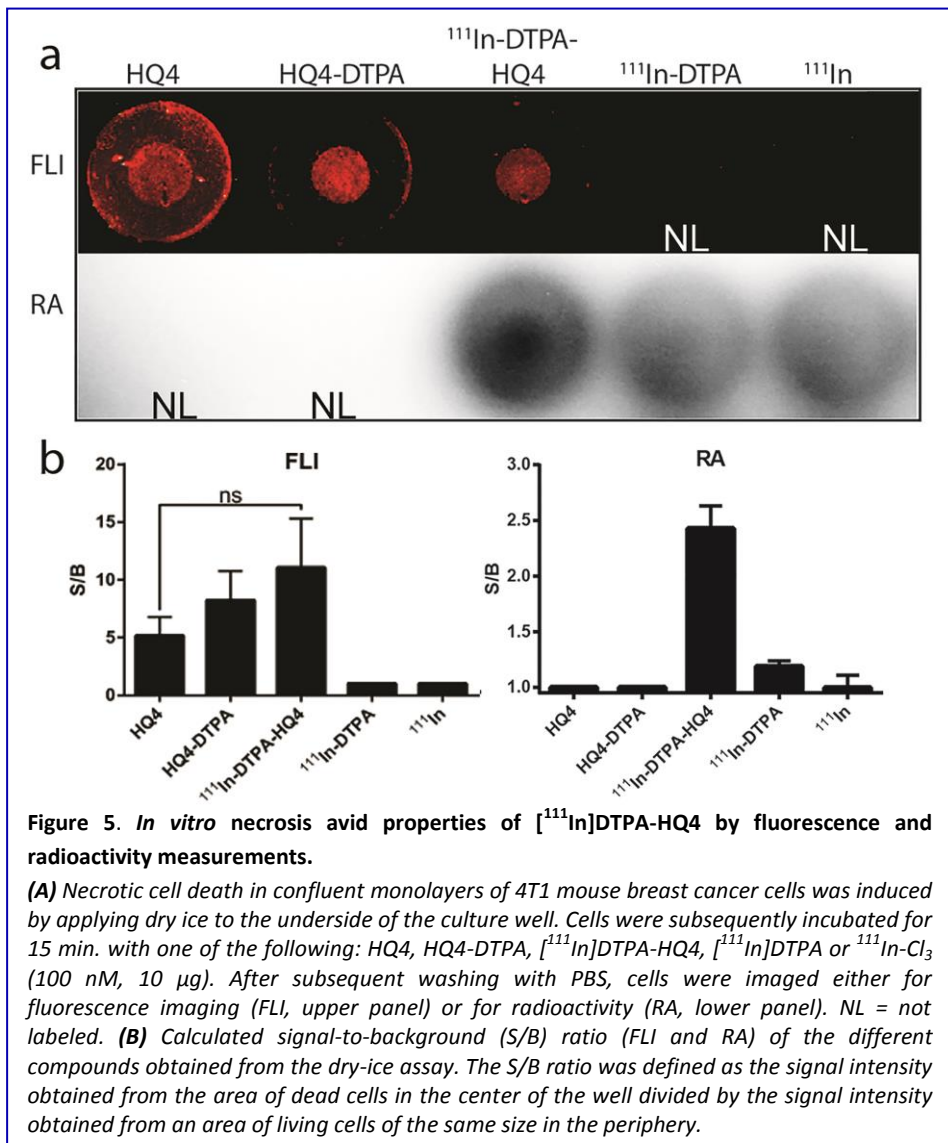
Figure 4. MTS cell viability assay of various agents.

Confluent cultures of 4T1 cells were incubated for 24hr with various concentrations HQ4, HQ4-DTPA, HQ5 or the natural anti-cancer compound Gambogic Acid (GA). Relative cell viability (%) was expressed as a percentage relative to the untreated control. HQ4, HQ4-DTPA and HQ5 did not affect cell viability, whereas, GA induced cell death with an IC₅₀ of around 6µM.

HQ4, HQ4-DTPA and HQ5 were examined in 24h cultures of 4T1 breast cancer cell and compared with the cytotoxic compound Gambogic acid (GA). In the dose range of 0 - 20 μM , none of the cyanine compounds affected cell viability. GA, however, dose dependently induced cell death with an IC50 of around 6 μM (see Fig. 4).

In vitro necrosis targeting properties of [^{111}In]DTPA-HQ4

The dry ice dead cell assay was performed to examine the necrosis avid properties of the entire conjugate [^{111}In]DTPA-HQ4 and the individual



components, HQ4 and HQ4-DTPA, respectively, *in vitro*. HQ4, HQ4-DTPA and [^{111}In]DTPA-HQ4 all strongly accumulated in the area of dead cells, as shown by fluorescence imaging (**Fig. 5A**). In addition, radioactive signal was obtained in areas of dead cells only when incubated with [^{111}In]DTPA-HQ4. In contrast, neither [^{111}In]DTPA nor free $^{111}\text{In-Cl}_3$ accumulated in the dead cells area, as indicated by RA measurements. **Figure 5B** shows quantifications of the fluorescent and radioactive signal-to-background (S/B) (dead cells vs living cells area) ratios for the five different compounds tested confirming that [^{111}In]DTPA-HQ4 retains fluorescence and radioactivity, as well as necrosis avidity with a S/B ratio of 11.1 and 2.4 respectively.

Necrosis targeting properties of [^{111}In]-DTPA-HQ4 in a 4T1 mouse tumor model of spontaneous necrosis

The necrosis targeting properties of [^{111}In]DTPA-HQ4 were evaluated in subcutaneous 4T1 breast tumor bearing mice, using SPECT and optical imaging. [^{111}In]DTPA-HQ4 (10 nmole, 30-35MBq) was injected intravenously (i.v.) into the tumor bearing mice, and *in vivo* SPECT and optical images were obtained 6, 24h, 48 and 72h, post injection (**Fig. 6A and B**). An increased retention of [^{111}In]DTPA-HQ4 in the tumors and in the metabolizing organs was observed over time with both optical imaging and SPECT.

To further assess the biodistribution of [^{111}In]DTPA-HQ4 in different organs, mice (n=3) were sacrificed at each time-point. Subsequently, radioactivity in various organs and body fluids was quantified (**Fig. 6C**). The measured radioactivity across different time points confirmed accumulation of radioactivity in the tumors (4.8 %ID/w), liver (3.3 %ID/w) and the kidneys (7.6 %ID/w) at 72hrs post injection. Finally, histological examination of the 4T1 tumors confirmed the presence of a large necrotic core, see **Figure 6D**.

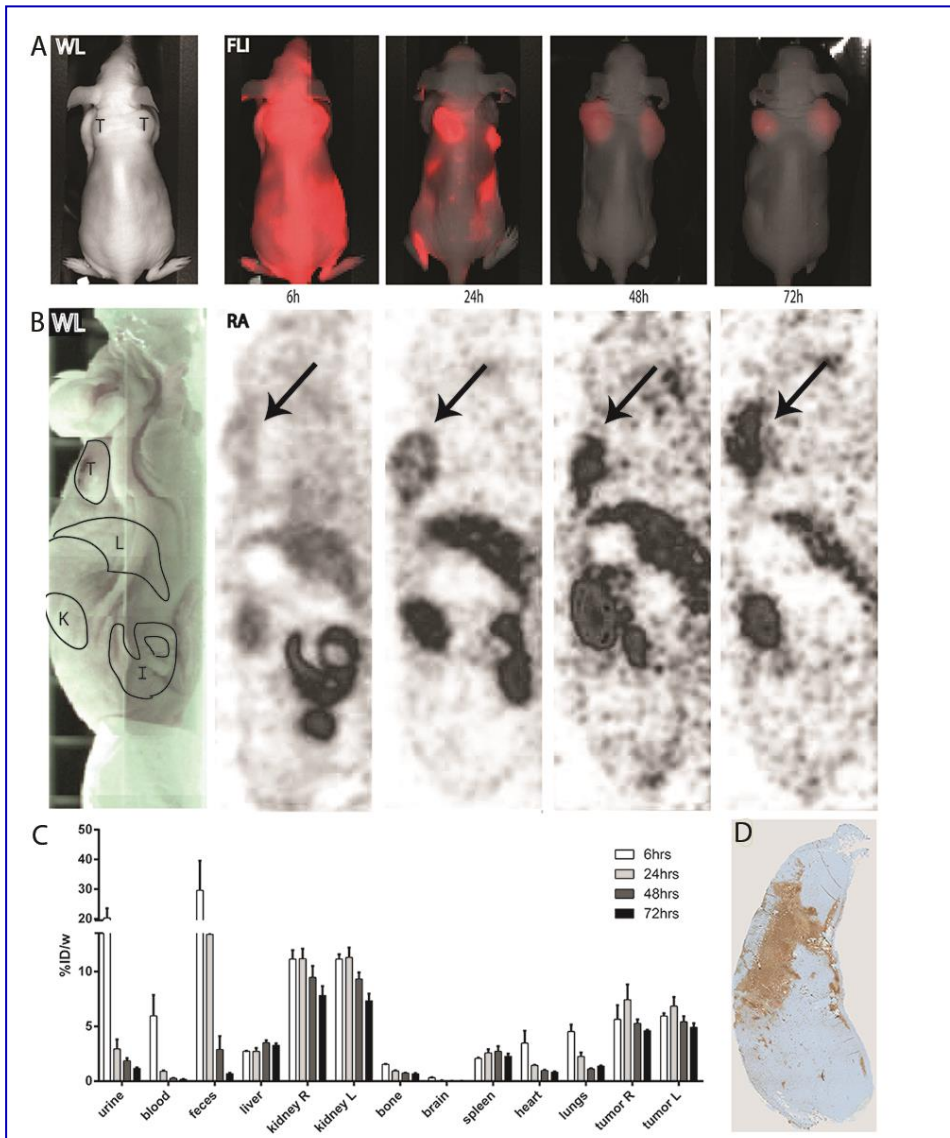


Figure 6. Optical imaging, SPECT and biodistribution of $[^{111}\text{In}]$ DTPA-HQ4 in 4T1 breast tumor bearing mice.

(A) Whole body FLI (coronal view) obtained 6-72h after tail vein injection of $[^{111}\text{In}]$ DTPA-HQ4 (10 nmole, 30-35 MBq). The white light image (WL) indicates the position of the mouse in the Pearl imager, from a dorsal point of view (T=tumor). The same device settings were applied to all FLI, rendering comparison between the different images possible. **(B)** Whole body SPECT images (sagittal view) obtained 6h-72h after tail vein injection of $[^{111}\text{In}]$ DTPA-HQ4 (10 nmole, 30-35 MBq). The white light image (WL) indicates the position of the mouse from a sagittal point of view, in the μ SPECT (RA); T=tumor, L=liver, K=kidney and I=intestine. Arrows indicate the tumor.

(C) Biodistribution of $[^{111}\text{In}]$ DTPA-HQ4 in 4T1 tumor bearing mice. 6h, 24h, 48h and 72h after probe injection, mice ($n=3$ per time point) were sacrificed and the organs, body fluids and tumors were dissected, weighed and measured for radioactivity in a gamma counter. At each time point, the amount of radioactivity in the organs is expressed as percentage of the injected dose divided by body weight (%ID/w). **(D)** TUNEL stained histological section of a representative 4T1 mouse breast tumor showing a large area of necrosis (brown).

Similarly, the biodistribution of the radiolabeled chelate [^{111}In]DTPA was examined in 4T1 tumor bearing mice 24h after i.v. injection of [^{111}In]DTPA (10 μg , 30-35 MBq). Mice (n=4) were euthanized and the internal organs and body fluids were removed to quantify remaining radioactivity (see Fig. 7A). Greatest accumulation of radioactivity was observed in the kidneys (5.0 %ID/w) and only relatively low values of radioactivity could be measured in other organs, body fluids and tumors (tumors; 0.5 %ID/w, liver 0.6 %ID/w).

Figure 7B, shows the measured amount of radioactivity in the mouse corpus at different time points after injection of [^{111}In]DTPA-HQ4 or [^{111}In]DTPA, expressed as the percentage of the total injected doses (%ID). It was found that 24h and 48h after injection of [^{111}In]DTPA-HQ4, respectively 38% and 35% of total injected dose was retained in the body, whereas, this was only 10% and 8%, for [^{111}In]DTPA.

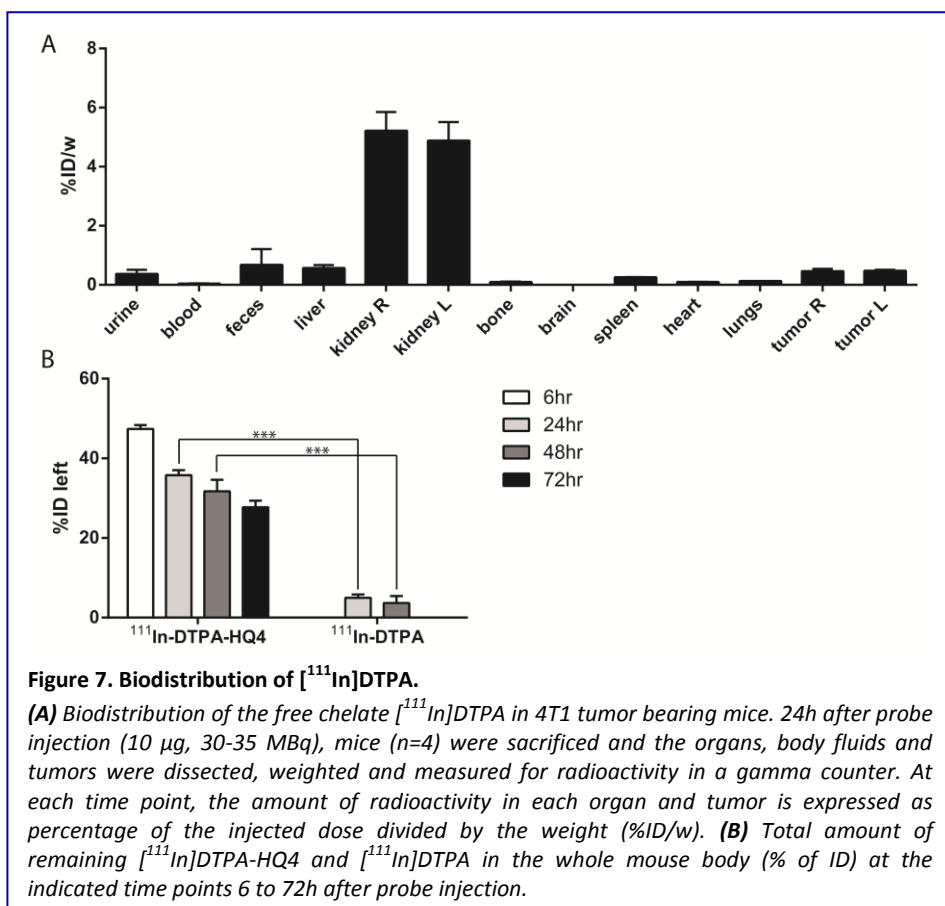
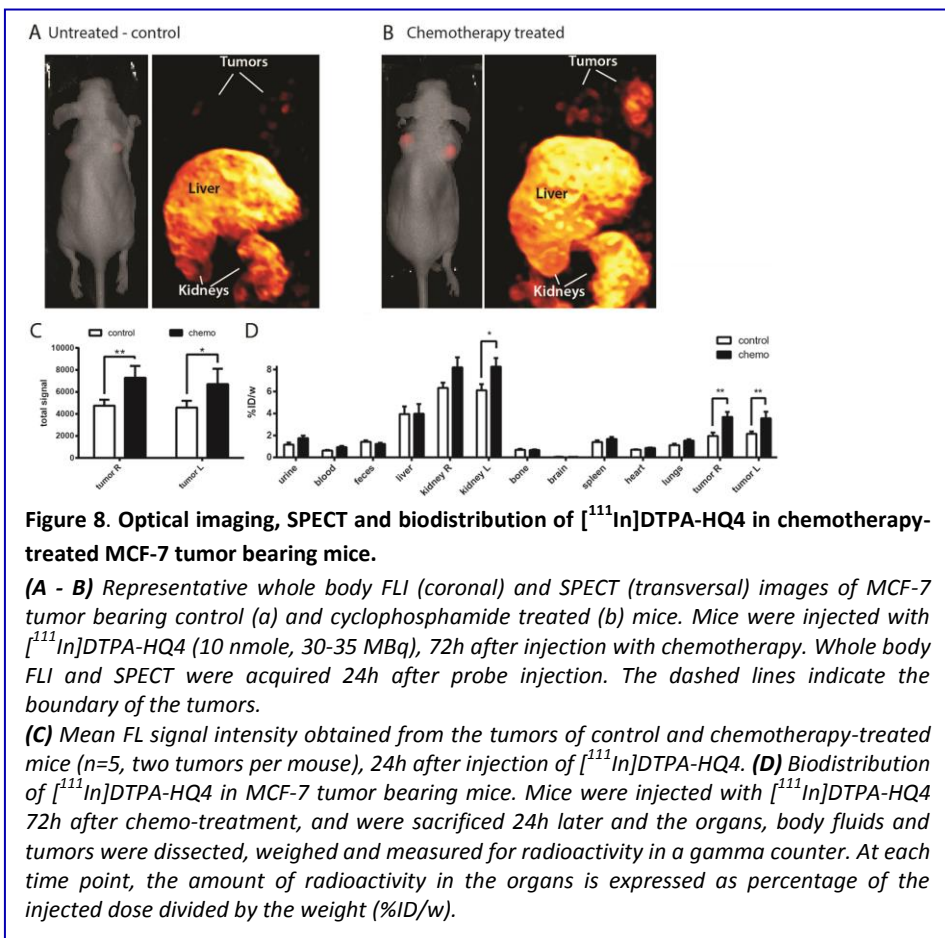


Figure 7. Biodistribution of [^{111}In]DTPA.

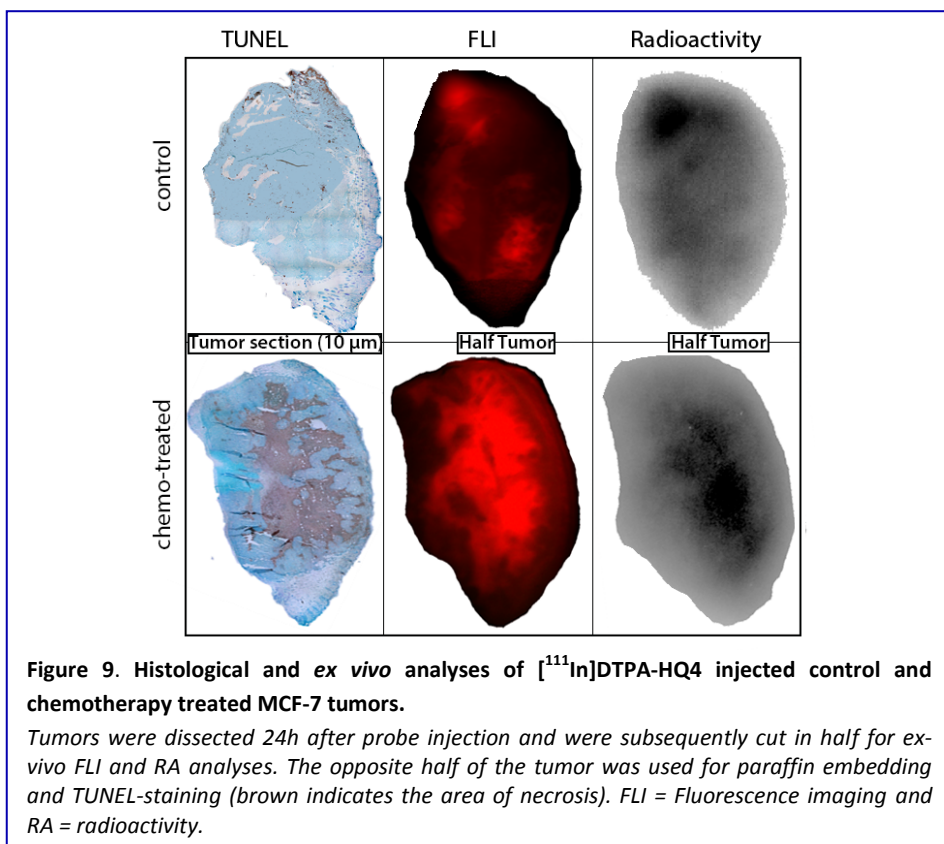
(A) Biodistribution of the free chelate [^{111}In]DTPA in 4T1 tumor bearing mice. 24h after probe injection (10 μg , 30-35 MBq), mice (n=4) were sacrificed and the organs, body fluids and tumors were dissected, weighted and measured for radioactivity in a gamma counter. At each time point, the amount of radioactivity in each organ and tumor is expressed as percentage of the injected dose divided by the weight (%ID/w). (B) Total amount of remaining [^{111}In]DTPA-HQ4 and [^{111}In]DTPA in the whole mouse body (% of ID) at the indicated time points 6 to 72h after probe injection.

SPECT and optical imaging of [¹¹¹In]DTPA-HQ4 in a MCF-7 mouse model of chemotherapy induced tumor necrosis

Using SPECT and optical imaging, we examined whether [¹¹¹In]DTPA-HQ4 could be employed to monitor chemotherapy induced tumor necrosis. For this, MCF-7 tumor bearing mice were treated with a single intraperitoneal (i.p.) injection of cyclophosphamide (265mg/kg)⁴⁴, followed by an i.v. injection of [¹¹¹In]DTPA-HQ4 (10 nmole, 30-35MBq) 72h later. 24h after injection of [¹¹¹In]DTPA-HQ4, whole body optical images and SPECT were obtained to assess its biodistribution. Both optical imaging and SPECT showed accumulation of [¹¹¹In]DTPA-HQ4 in cyclophosphamide treated tumors as compared to untreated tumors (**Fig. 8A** and **B**). **Figure 8C** shows quantification of the fluorescent signals obtained from the tumors, 24h after probe injection. A significant increase in tumor fluorescent signal intensity was observed in mice that were treated with chemotherapy as compared to untreated controls (ratio = 1.8:1.0, p= 0.0011).



Biodistribution study based on quantification of radioactivity in various organs further demonstrated higher amount of radioactivity in chemotherapy treated tumors compared to untreated controls. The average %ID/w was 1.85 for the control tumors vs 4.02 for the chemo-treated tumors (**Fig. 8D**). In addition, a significantly higher amount (1.4-fold) of radioactivity was observed in left kidneys of the chemotherapy-treated mice as compared to controls. Finally, tumors of chemotherapy-treated and control mice, which were injected with [^{111}In]DTPA-HQ4 (10 nmole, 30-35 MBq), were dissected and cut in half to perform *ex-vivo* fluorescence and radioactivity analysis. In addition, the opposite half of the tumor was processed for paraffin embedding and histological analysis. As shown in **Figure 9**, the TUNEL stained section of the untreated control tumor showed very little necrotic tissue, whereas the chemotherapy-treated tumor contained a large area of necrotic tissue (brown staining). Notably, the TUNEL staining showed co-localization with both fluorescence and radioactivity signals in tumors, confirming the specific increased necrosis retention property of [^{111}In]DTPA-HQ4. For comparison all the settings used for the different images are similar.



Discussion

Over the last two decades, several attempts have been made to exploit disease and/or therapy induced tumor necrosis as a diagnostic and/or prognostic biomarker of disease and to utilize necrotic tissue as a target for drug delivery. The existing necrosis imaging agents can be divided in two different groups; (non-) specific CT and MR contrast agents to enhance the natural signal and the other group consists out of mostly radiolabeled necrosis avid contrast agents (NACAs) that specifically target necrotic tissue. The latter can also be employed for therapeutic purposes e.g. when radiolabeled with ^{131}I iodine^{2-10,13,15,23,45-49}. It is expected that the non-specific necrosis contrast agents will fall into abeyance when compounds with high necrosis specificity become clinically available. However, thus far, only the ^{131}I iodine conjugated Tumor Necrosis Targeting Therapy monoclonal antibody (TNT-3), licensed by Peregrine Pharmaceuticals, reached the clinical trials for therapeutic use^{13,21}. This antibody, under the brand name CotaraTM, has been examined in clinical trials for treatment of Glioblastoma Multiforma. However, although encouraging results have been published on the website of the manufacturer in December 2012, no follow-up studies have been reported since⁵⁰. In addition, the necrosis avid photosensitizer Hypericin, under the brand name Oncocidia, is also under investigation to enter clinical trials^{14,51,52}. Although proof of concept has been shown for both approaches, both compounds, as mentioned earlier, suffer from major drawbacks which hampers their clinical translation.

To overcome the limitations associated with the size and possible immunogenicity of antibodies, the photo-toxicity, problems with solubility and ability to aggregate, a simple, injectable and non-toxic agent that displays specific necrosis avidity is required. Recently, we demonstrated that two non-toxic constituents of the group of NIRF cyanine dyes, IRDye800CW and HQ5 carboxylate, the former being commonly used as an optical probe for biomolecular labeling^{53,54}, display strong and specific necrosis avid properties *in vitro* as well as in tumor bearing mice²³. In this study, the increased retention of NIRF cyanine dyes in tumor necrosis was examined using whole body fluorescence imaging. Although whole body optical imaging is suitable for use in small animals, it is often insufficient for assessments of deep tissues in the human body, due to the limited tissue penetration depth of NIRF light. In order to seek for potential clinical applications for our newly discovered necrosis avid cyanines, we examined the possibility to radiolabel it for *in vivo*

nuclear imaging by conjugating to a chelator^{55,56}. To render HQ4 applicable for SPECT we first conjugated HQ4 to the chelate DTPA with a linker molecule, and subsequently radiolabeled with $^{111}\text{In-Cl}_3$. Following the synthesis and purification procedures, purity of 98% was achieved. Thus, we created a molecule that targets necrosis and can be imaged using both NIRF and SPECT.

We demonstrated *in vitro* that [^{111}In]DTPA-HQ4, like unconjugated HQ4, appears to specifically bound to dead cells after washing. Our findings, in the dry ice assay, show that the specificity of [^{111}In]DTPA-HQ4 for necrotic cells was solely due to the presence of the HQ4 molecule, as the radiolabeled chelate [^{111}In]DTPA alone and free $^{111}\text{In-Cl}_3$ did not show to bind to the dead cells. Although DTPA conjugation is likely to change the chemical and physico-chemical properties of HQ4, for example by increasing its overall hydrophilicity⁵⁷, it retained its necrosis avid- and fluorescent properties. We observed a clear difference in the signal-to-background (S/B) ratio of [^{111}In]DTPA-HQ4 between fluorescence- and radioactivity measurements. The reason for this discrepancy is unclear, but may involve environmental conditions that specifically affect the fluorescent properties of the molecule. Previously, Jiskoot et. al⁵⁸ reviewed the fluorescence properties of extrinsic dyes, which are strongly influenced by their environment (hydrophilic/hydrophobic or differences in pH) and/or by interactions with proteins. Such factors may also influence fluorescence signal intensity of HQ4 in an environment of living cells compared to in an environment of dead cells. However, such environmental dependent signal intensity influences will not occur when a radiolabel, offering a quantitative readout, is utilized. Nevertheless, the observed S/B ratio of 2.5, obtained with radioactivity measurements, is theoretically sufficient for clinical translation⁵⁹. Additional studies that determine the relationship between time, probe concentration, and S/B ratio could help to optimize the sensitivity of the measurements. Furthermore, none of the cyanine dyes, including HQ4-DTPA, showed any acute *in vitro* toxicity in cultures of 4T1 cells. Even at the highest concentration of 20uM (during 24h), which is 200-fold higher compared to the concentration used to image dead cells *in vitro*, cell viability remained unaffected. Collectively, our *in vitro* study revealed that DTPA conjugation is not deleterious to the necrosis avid properties of HQ4 and the lack of toxicity encouraging further studies with the aim of its clinical translation. Further investigations are warranted concerning the mechanism of interaction of the DTPA conjugated cyanine to specific proteins in necrotic cells. In the paper of

Xie et. al.²³ we showed that HQ5, a close cyanine analogue of HQ4, specifically accumulated in necrotic cells and not in apoptotic cells. Moreover we have shown that HQ5 does not co-localize with F4/80 macrophage staining in an around the tumor, indicative of inflammation. Nevertheless, we did not yet examine these specific mechanistic properties for HQ4..

Using *in vivo* whole body optical imaging, SPECT, and *ex vivo* analysis, we confirmed the observed *in vitro* necrosis avid properties of [¹¹¹In]DTPA-HQ4 in two tumor models: 4T1 mouse breast cancer tumor model of spontaneous necrosis and MCF-7 human breast cancer tumor model of chemotherapy induced tumor necrosis. MCF-7 tumor model was selected to assess chemotherapy-induced necrosis due to its slow growth kinetics. MCF-7 tumor cells have a population doubling time (PDT) of approximately 38h *in vitro*⁶⁰, thus representing a slow-growing tumor. This is in contrast to 4T1-cells, PDT +/- 12h⁶¹, which develop necrotic cores spontaneously, and to EL4-cells, PDT +/- 17h⁶², used in the previous paper²³. Since MCF-7 cells hardly develop spontaneous necrosis during their growth, necrosis induced by chemotherapy is more evident and can be determined with higher accuracy. Moreover, MCF-7 cells are of human origin, which may also more accurately mimic the clinical situation⁶³.

In both mouse tumor models, the acquired optical imaging and SPECT results over time, provided information on the pharmacokinetic profile of [¹¹¹In]DTPA-HQ4. In the model of spontaneous tumor necrosis, necrotic areas in the tumor were clearly delineated using optical imaging and SPECT. No clear specific tissue interactions could be detected 6h after injection, probably due to high quantities of unbound circulating probe in the blood at this early time point. The amount of radioactivity that retained in the 4T1 tumors remained approximately equal over time, while, it declined in most organs and body fluids, resulting in a relative increase in tumor signal intensity inside the tumor at later time points. In the chemotherapy-induced tumor necrosis model, the specific targeting of [¹¹¹In]DTPA-HQ4 to necrotic areas of MCF-7 tumors was confirmed histologically using TUNEL staining. In this model we also observed that the kidneys of the chemotherapy-treated mice retained more radioactivity than in untreated mice. The reason for this is unknown, but it might be speculated that some necrosis may develop due to cyclophosphamide induced renal oxidative stress which leads to peroxidative damage to the kidneys⁶⁴.

Finally, we compared the biodistribution and clearance rate of [¹¹¹In]DTPA-HQ4 with that of the free labeled chelate ([¹¹¹In]DTPA). We observed that both

the biodistribution and the excretion rate of the two compounds were vastly different. 24h after probe injection, [^{111}In]DTPA was mainly retained in the kidneys and could hardly be detected in other organs or in the tumors, confirming our *in vitro* findings of a lack of tumor necrosis specificity. The observed accumulation of [^{111}In]DTPA in the kidneys confirms findings of Boswell and colleagues⁶⁵ who also reported predominant clearance of this hydrophilic compound via this excretion route. Moreover, not only the organ distribution of these two compounds was dissimilar, the clearance rate of [^{111}In]DTPA was about 8-fold faster than that of [^{111}In]DTPA-HQ4. Combined, these findings indicate that both the pharmacokinetics and the tissue targeting properties of [^{111}In]DTPA-HQ4 and [^{111}In]DTPA are largely different and strengthen the notion that the cyanine HQ4 governs the overall necrosis avid properties of the [^{111}In]DTPA-HQ4 molecule.

In summary, we successfully yielded a new necrosis avid SPECT radiotracer by conjugating the necrosis avid cyanine HQ4 to DTPA, followed by radiolabeling with $^{111}\text{In-Cl}_3$. We showed that, after DTPA conjugation, this newly synthesized radiotracer retained its specific necrosis targeting properties *in vitro* and *in vivo* in mouse models of spontaneous and therapy induced tumor necrosis. The advantages of the small molecule [^{111}In]DTPA-HQ4 include; high water solubility, NIR property that enables deep penetration into tissues, lack of photo-toxicity, and low production costs. Therefore, the necrosis avid radiotracer [^{111}In]DTPA-HQ4 has the potential to be clinically translated for diagnostic-prognostic purposes and to predict early treatment outcome of anti-cancer treatments.

Acknowledgments

This work was supported by project grants from TI Pharma (Project D4-603), the EU Seventh Framework Program: FP7-PEOPLE-2013-IAPP (612360 – BRAINPATH), H2020-MSCA-RISE grant number 644373 – PRISAR. K.B. is supported by a FP7-PEOPLE-2013-IEF grant (625798 Image-Guided Surgery). HQTM compounds are a trade mark of Ilumicare BV, Rotterdam, The Netherlands who also financially supported part of the studies. We acknowledge the technical assistance of Henny Bloys-de Groot in preparing the immunohistochemistry sections. We would further like to acknowledge the generous gift of Π.pmod Biomedical Image Quantification to be able to use their software to reconstruct our μSPECT scans.

References

1. de Bruin EC, Medema JP. Apoptosis and non-apoptotic deaths in cancer development and treatment response. *Cancer Treat Rev.* 2008;34(8):737-749.
2. Venkatramani R, Wang L, Malvar J, et al. Tumor necrosis predicts survival following neo-adjuvant chemotherapy for hepatoblastoma. *Pediatr Blood Cancer.* 2012;59(3):493-498.
3. Hiraoka N, Ino Y, Sekine S, et al. Tumour necrosis is a postoperative prognostic marker for pancreatic cancer patients with a high interobserver reproducibility in histological evaluation. *British journal of cancer.* 2010;103(7):1057-1065.
4. Kato T, Kameoka S, Kimura T, Tanaka S, Nishikawa T, Kobayashi M. p53, mitosis, apoptosis and necrosis as prognostic indicators of long-term survival in breast cancer. *Anticancer Res.* 2002;22(2B):1105-1112.
5. Maiorano E, Regan MM, Viale G, et al. Prognostic and predictive impact of central necrosis and fibrosis in early breast cancer: results from two International Breast Cancer Study Group randomized trials of chemoendocrine adjuvant therapy. *Breast cancer research and treatment.* 2010;121(1):211-218.
6. Park SY, Lee HS, Jang HJ, Lee GK, Chung KY, Zo JI. Tumor necrosis as a prognostic factor for stage IA non-small cell lung cancer. *The Annals of thoracic surgery.* 2011;91(6):1668-1673.
7. Pichler M, Hutterer GC, Chromecki TF, et al. Histologic tumor necrosis is an independent prognostic indicator for clear cell and papillary renal cell carcinoma. *American journal of clinical pathology.* 2012;137(2):283-289.
8. Pollheimer MJ, Kornprat P, Lindtner RA, et al. Tumor necrosis is a new promising prognostic factor in colorectal cancer. *Human pathology.* 2010;41(12):1749-1757.
9. Richards CH, Roxburgh CS, Anderson JH, et al. Prognostic value of tumour necrosis and host inflammatory responses in colorectal cancer. *The British journal of surgery.* 2012;99(2):287-294.
10. Uhl M, Saueressig U, Koehler G, et al. Evaluation of tumour necrosis during chemotherapy with diffusion-weighted MR imaging: preliminary results in osteosarcomas. *Pediatric radiology.* 2006;36(12):1306-1311.
11. Silva MT. Secondary necrosis: the natural outcome of the complete apoptotic program. *FEBS Lett.* 2010;584(22):4491-4499.
12. Kepp O, Galluzzi L, Lipinski M, Yuan J, Kroemer G. Cell death assays for drug discovery. *Nature reviews Drug discovery.* 2011;10(3):221-237.
13. Epstein AL, Chen FM, Taylor CR. A novel method for the detection of necrotic lesions in human cancers. *Cancer research.* 1988;48(20):5842-5848.
14. Cona MM, de Witte P, Verbruggen A, Ni Y. An overview of translational (radio)pharmaceutical research related to certain oncological and non-oncological applications. *World journal of methodology.* 2013;3(4):45-64.
15. Jiang B, Wang J, Ni Y, Chen F. Necrosis avidity: a newly discovered feature of hypericin and its preclinical applications in necrosis imaging. *Theranostics.* 2013;3(9):667-676.
16. Hritz J, Kascakova S, Ulicny J, Miskovsky P. Influence of structure of human, rat, and bovine serum albumins on binding properties of photoactive drug hypericin. *Biopolymers.* 2002;67(4-5):251-254.

17. Miskovsky P. Hypericin--a new antiviral and antitumor photosensitizer: mechanism of action and interaction with biological macromolecules. *Current drug targets*. 2002;3(1):55-84.
18. Solar P, Cavarga I, Hofmanova J, et al. Effect of acetazolamide on hypericin photocytotoxicity. *Planta medica*. 2002;68(7):658-660.
19. Wang H, Cao C, Li B, et al. Immunogenicity of Iodine 131 chimeric tumor necrosis therapy monoclonal antibody in advanced lung cancer patients. *Cancer immunology, immunotherapy : CII*. 2008;57(5):677-684.
20. Ni Y, Bormans G, Chen F, Verbruggen A, Marchal G. Necrosis avid contrast agents: functional similarity versus structural diversity. *Investigative radiology*. 2005;40(8):526-535.
21. Hdeib A, Sloan A. Targeted radioimmunotherapy: the role of (1)(3)(1)I-chTNT-1/B mAb (Cotara) for treatment of high-grade gliomas. *Future oncology*. 2012;8(6):659-669.
22. Cona MM, Alpizar YA, Li J, et al. Radioiodinated hypericin: its biodistribution, necrosis avidity and therapeutic efficacy are influenced by formulation. *Pharmaceutical research*. 2014;31(2):278-290.
23. Xie B, Stammes MA, van Driel PB, et al. Necrosis avid near infrared fluorescent cyanines for imaging cell death and their use to monitor therapeutic efficacy in mouse tumor models. *Oncotarget*. 2015.
24. Boonstra MC, van Driel PB, van Willigen DM, et al. uPAR-targeted multimodal tracer for pre- and intraoperative imaging in cancer surgery. *Oncotarget*. 2015;6(16):14260-14273.
25. He H, Tu X, Zhang J, et al. A novel antibody targeting CD24 and hepatocellular carcinoma in vivo by near-infrared fluorescence imaging. *Immunobiology*. 2015;220(12):1328-1336.
26. Verbeek FP, van der Vorst JR, Tummers QR, et al. Near-infrared fluorescence imaging of both colorectal cancer and ureters using a low-dose integrin targeted probe. *Annals of surgical oncology*. 2014;21 Suppl 4:S528-537.
27. Warram JM, de Boer E, Sorace AG, et al. Antibody-based imaging strategies for cancer. *Cancer metastasis reviews*. 2014;33(2-3):809-822.
28. Sato K, Gorka AP, Nagaya T, et al. Role of Fluorophore Charge on the In Vivo Optical Imaging Properties of Near-Infrared Cyanine Dye/Monoclonal Antibody Conjugates. *Bioconjugate chemistry*. 2015.
29. Berezin MY, Guo K, Akers W, et al. Rational approach to select small peptide molecular probes labeled with fluorescent cyanine dyes for in vivo optical imaging. *Biochemistry*. 2011;50(13):2691-2700.
30. Kroemer G, Galluzzi L, Brenner C. Mitochondrial membrane permeabilization in cell death. *Physiological reviews*. 2007;87(1):99-163.
31. Proskuryakov SY, Konoplyannikov AG, Gabai VL. Necrosis: a specific form of programmed cell death? *Experimental cell research*. 2003;283(1):1-16.
32. Majno G, Joris I. Apoptosis, oncosis, and necrosis. An overview of cell death. *The American journal of pathology*. 1995;146(1):3-15.
33. Keereweer S, Van Driel PB, Snoeks TJ, et al. Optical image-guided cancer surgery: challenges and limitations. *Clin Cancer Res*. 2013;19(14):3745-3754.
34. Pleijhuis R, Timmermans A, De Jong J, De Boer E, Ntziachristos V, Van Dam G. Tissue-simulating phantoms for assessing potential near-infrared fluorescence

- imaging applications in breast cancer surgery. *Journal of visualized experiments : JoVE*. 2014(91):51776.
35. Paulus A, Desai P, Carney B, et al. Development of a clickable bimodal fluorescent/PET probe for in vivo imaging. *EJNMMI research*. 2015;5(1):120.
 36. Seibold U, Wangler B, Schirmmacher R, Wangler C. Bimodal imaging probes for combined PET and OI: recent developments and future directions for hybrid agent development. *BioMed research international*. 2014;2014:153741.
 37. Morais M, Campello MP, Xavier C, et al. Radiolabeled mannosylated dextran derivatives bearing an NIR-fluorophore for sentinel lymph node imaging. *Bioconjugate chemistry*. 2014;25(11):1963-1970.
 38. Zhu H, Zhao J, Lin X, Hong Y, Li C, Yang Z. Design, synthesis and evaluation of dual-modality glyco-nanoparticles for tumor imaging. *Molecules*. 2013;18(6):6425-6438.
 39. Majonis D, Ornatsky O, Weinrich D, Winnik MA. Dual-purpose polymer labels for fluorescent and mass cytometric affinity bioassays. *Biomacromolecules*. 2013;14(5):1503-1513.
 40. Xie BW, Park D, Van Beek ER, et al. Optical imaging of cell death in traumatic brain injury using a heat shock protein-90 alkylator. *Cell death & disease*. 2013;4:e473.
 41. Brom M, Joosten L, Oyen WJ, Gotthardt M, Boerman OC. Improved labelling of DTPA- and DOTA-conjugated peptides and antibodies with ¹¹¹In in HEPES and MES buffer. *EJNMMI research*. 2012;2:4.
 42. Goorden MC, Beekman FJ. High-resolution tomography of positron emitters with clustered pinhole SPECT. *Physics in medicine and biology*. 2010;55(5):1265-1277.
 43. Branderhorst W, Vastenhouw B, Beekman FJ. Pixel-based subsets for rapid multi-pinhole SPECT reconstruction. *Physics in medicine and biology*. 2010;55(7):2023-2034.
 44. Paine-Murrieta GD, Taylor CW, Curtis RA, et al. Human tumor models in the severe combined immune deficient (scid) mouse. *Cancer chemotherapy and pharmacology*. 1997;40(3):209-214.
 45. Prinsen K, Jin L, Vunckx K, et al. Radiolabeling and preliminary biological evaluation of a (99m)Tc(CO)(3) labeled 3,3'-(benzylidene)-bis-(1H-indole-2-carbohydrazide) derivative as a potential SPECT tracer for in vivo visualization of necrosis. *Bioorganic & medicinal chemistry letters*. 2011;21(1):502-505.
 46. Van Walleghe DM, Parseghian MH. Toxicity and biodistribution of an iodine-131-radiolabelled tumour necrosis-targeting antibody in non-tumour-bearing domestic felines. *Veterinary and comparative oncology*. 2006;4(1):9-20.
 47. Verma N, Cowperthwaite MC, Burnett MG, Markey MK. Differentiating tumor recurrence from treatment necrosis: a review of neuro-oncologic imaging strategies. *Neuro-oncology*. 2013;15(5):515-534.
 48. Murphy KP, O'Connor OJ, Maher MM. Updated imaging nomenclature for acute pancreatitis. *AJR American journal of roentgenology*. 2014;203(5):W464-469.
 49. Carlsson M, Arheden H, Higgins CB, Saeed M. Magnetic resonance imaging as a potential gold standard for infarct quantification. *Journal of electrocardiology*. 2008;41(6):614-620.
 50. Pharmaceuticals P. Cotara Oncology. Accessed October 26, 2015.

51. Ni Y. Abstract 1767: Oncocidia: a small molecule dual targeting pan-anticancer theragnostic strategy. abstract presented at Proceedings of the 105th Annual Meeting of the American Association for Cancer Research; 2014 Apr 5-9, 2014; San Diego, CA. Philadelphia (PA).
52. Cona MM, Li J, Feng Y, et al. Targetability and biodistribution of radioiodinated hypericin: comparison between microdosing and carrier-added preparations. *Anti-cancer agents in medicinal chemistry*. 2014;14(6):852-861.
53. Krabbendam R, Pool M, de Vries LG, Offerhaus HL, Herek JL, Otto C. Hybrid imaging of fluorescently labeled cancer drugs and label-free four-wave mixing microscopy of cancer cells and tissues. *Journal of biomedical optics*. 2015;20(8):86006.
54. Rijpkema M, Bos DL, Cornelissen AS, et al. Optimization of Dual-Labeled Antibodies for Targeted Intraoperative Imaging of Tumors. *Molecular imaging*. 2015;14:348-355.
55. Sosabowski JK, Mather SJ. Conjugation of DOTA-like chelating agents to peptides and radiolabeling with trivalent metallic isotopes. *Nature protocols*. 2006;1(2):972-976.
56. Cooper MS, Sabbah E, Mather SJ. Conjugation of chelating agents to proteins and radiolabeling with trivalent metallic isotopes. *Nature protocols*. 2006;1(1):314-317.
57. Adams PC, Lin E, Barber KR, Grant CW. Enhanced biliary iron excretion with amphiphilic diethylenetriaminepentaacetic acid. *Hepatology*. 1991;14(6):1230-1234.
58. Hawe A, Sutter M, Jiskoot W. Extrinsic fluorescent dyes as tools for protein characterization. *Pharmaceutical research*. 2008;25(7):1487-1499.
59. Frangioni JV. New technologies for human cancer imaging. *Journal of clinical oncology : official journal of the American Society of Clinical Oncology*. 2008;26(24):4012-4021.
60. ATCC. SOP: Thawing, Propagating and Cryopreserving of NCI-PBCF-HTB22 (MCF-7). 2012.
61. Kim JB, Urban K, Cochran E, et al. Non-invasive detection of a small number of bioluminescent cancer cells in vivo. *PloS one*. 2010;5(2):e9364.
62. Koo GC, Huang C, Camacho R, et al. Immune enhancing effect of a growth hormone secretagogue. *Journal of immunology*. 2001;166(6):4195-4201.
63. Friberg S, Mattson S. On the growth rates of human malignant tumors: implications for medical decision making. *Journal of surgical oncology*. 1997;65(4):284-297.
64. Rehman MU, Tahir M, Ali F, et al. Cyclophosphamide-induced nephrotoxicity, genotoxicity, and damage in kidney genomic DNA of Swiss albino mice: the protective effect of Ellagic acid. *Molecular and cellular biochemistry*. 2012;365(1-2):119-127.
65. Boswell CA, Ferl GZ, Mundo EE, et al. Effects of anti-VEGF on predicted antibody biodistribution: roles of vascular volume, interstitial volume, and blood flow. *PloS one*. 2011;6(3):e17874.